



CHORUS

This is the accepted manuscript made available via CHORUS. The article has been published as:

Structural and dynamical properties of liquid $\text{Cu}_{80}\text{Si}_{20}$ alloy studied experimentally and by ab initio molecular dynamics simulations

S. Wu, M. J. Kramer, X. W. Fang, S. Y. Wang, C. Z. Wang, K. M. Ho, Z. J. Ding, and L. Y. Chen

Phys. Rev. B **84**, 134208 — Published 24 October 2011

DOI: [10.1103/PhysRevB.84.134208](https://doi.org/10.1103/PhysRevB.84.134208)

Structural and Dynamical Properties of Liquid $\text{Cu}_{80}\text{Si}_{20}$ Alloy by Experimental and *ab initio* Molecular Dynamics Simulation Studies

S. Wu,¹ M. J. Kramer,² X. W. Fang,^{2,3} S. Y. Wang,^{1,2,*} C. Z. Wang,^{2,#} K. M. Ho,²
Z. J. Ding,³ and L. Y. Chen¹

¹ *Department of Optical Science and Engineering, Fudan University, Shanghai 200433, China*

² *Ames Laboratory, U. S. Department of Energy and Department of Physics and Astronomy,
Iowa State University, Ames, Iowa 50011, USA*

³ *Hefei National Laboratory for Physical Sciences at Microscale and Department of Physics,
University of Science and Technology of China, Hefei, Anhui, 230026, China*

The local structures and dynamical properties of liquid $\text{Cu}_{80}\text{Si}_{20}$ alloy have been studied by X-ray diffraction and *ab initio* molecular dynamics (MD) simulations. The pair-correlation functions and the structure factors derived from the three dimensional coordinates of the MD configurations agree well with the experimental results. The local structure of the liquids is analyzed using Honeycutt-Andersen (HA) indices, Voronoi tessellation, and an atomic cluster alignment method. The Honeycutt-Andersen indices analysis shows that the pentagonal bipyramid, a fragment of an icosahedron, plays a dominant role in the short-range order (SRO) of the $\text{Cu}_{80}\text{Si}_{20}$ liquid. The HA indices corresponding to the pentagonal bipyramid increases dramatically with decreasing temperature. Voronoi tessellation analysis indicates while the liquid does exhibit a strong icosahedral SRO, FCC-like SRO is also measureable. The results from Voronoi tessellation analysis are further confirmed using the recently developed atomic cluster alignment method. Finally, self-diffusion constants as the function of temperature for both Cu and Si species are calculated.

Keywords: X-ray diffraction, *Ab initio* molecular dynamics, Local structure, Liquid, CuSi

PACS number(s): 61.05.cp, 61.20.Ja, 61.25.Mv, 71.15.Pd

I. INTRODUCTION

The chemical and structural order which occurs in a molten alloy as it is cooled or conversely, the amorphous state as it is heated above the glass transition, involve complex atomic rearrangements. While the end-point of the transformation process, i.e., crystalline nano/microstructure, can be well defined through electron microscopy and X-ray diffraction methods, both the starting point and pathways are ill defined from an atomic structure viewpoint. Investigations into the chemical and topological ordering in liquid alloys prior to crystallization are now assessable through neutron¹ and high energy X-ray scattering,^{2,3} but these experimental studies can provide only one-dimensional correlation function of the structure of a liquid while higher order correlations are necessary to fully describe a disordered system. Nevertheless, such experimental shortcoming can be compensated by modern computational methods, such as molecular dynamics⁴ and reverse Monte Carlo⁵ simulations. Using the computational approaches, especially the highly accurate *ab initio* molecular dynamics simulations, a detailed structure of the liquid alloy at the atomistic level can be obtained. Using experiments to validate *ab initio* MD models allows for greater confidence in the reliability of structural and dynamical properties of metallic liquids derived from the simulations.

In this paper, the structural and dynamical properties of Cu₈₀Si₂₀ liquid alloy, in which the concentration is very close to the eutectic point of the Cu-Si system where the melting temperature of the system is usually lowest and no phase separation or precipitation occurs before the solidification,⁶ are investigated by X-ray diffraction and *ab initio* molecular dynamics simulations. While the Cu and Si both form simple cubic crystals, the Cu rich eutectic contains a large number of complex stable and metastable crystalline phases in the binary system and a high degree of solubility for Si in Cu. The composition chosen lies near the deep eutectic around

which the intermetallic compounds form. In contrast, Ag and Au form no compounds with Si and have limited solubility even though they have similar electronic structures to Cu.⁷ This is an interesting system which to compare the local order in the liquid to that of the potential nucleating phases in this system. The atomic structures obtained from the *ab initio* MD simulations are analyzed using Honeycutt-Andersen (HA) indices, Voronoi tessellation, and a newly developed atomic cluster alignment method. The self-diffusion is then analyzed as a function of temperature by monitoring the mean-squared atomic displacements.

The remaining part of this paper is organized as follows: The experimental and computational details will be described in the next section. The results obtained from the simulations will be shown and discussed in Section III. Hereafter, the detailed discussions on the short-range order (SRO) and dynamical properties of $\text{Cu}_{80}\text{Si}_{20}$ are given. Finally, conclusions are made in Section IV.

II. EXPERIMENTAL AND COMPUTATIONAL DETAILS

High-energy synchrotron X-ray diffraction (HEXRD) was used to study the liquid $\text{Cu}_{80}\text{Si}_{20}$ alloy at 4 temperatures, 1250 K, 1210 K, 1175 K, and 1140 K, respectively. The melting point of this alloy is approximately 1093 K.⁶ These samples were cast from appropriate mixtures of high-purity Cu (99.99%) and Si (99.99%) and were sealed in thin-walled 1×2 mm diameter quartz channels and sealed in ≈ 6.7 MPa (≈ 500 torr) Ar. Then, the samples were uniformly heated using a cylindrical Pt-Rh wound resistance furnace with a very low temperature gradient.⁸ It was observed that the samples could be heated to ≈ 1400 K before reaction with the container occurred. The HEXRD studies were performed at the MUCAT 6-IDD beamline at the Advanced Photon Source using the energy of 97.84 keV, corresponding to a wavelength (λ) of 0.12643 Å. Silicon double-crystal monochromators were applied to select the wavelength. The

diffraction data were collected in transmission using a MAR345 image plate detector at a distance of 0.425 m, providing a usable range in the wave momentum number ($q=4\pi\sin\theta/\lambda$) of $\approx 20 \text{ \AA}^{-1}$. The diffracted intensity as a function of q was derived by integrating around the Debye rings of the exposed image plate. The wavelength was determined using an energy dispersive detector. The sample to detector distance was determined using NIST Si Standard Reference Material 640C. The required geometric corrections for misalignment of the detector relative to the beam normal were performed using FIT2D.⁹ The data were then converted to the total structure factor, $S(q)$, and Fourier transform to the reduced distribution function $g(r)$ by standard procedures.^{10, 11} An acquisition time of 60 s provides high quality data with signal to noise comparable to neutron data sets whose acquisition times are 1 to 2 orders of magnitude longer in duration.¹²

The *ab initio* MD simulations of $\text{Cu}_{80}\text{Si}_{20}$ liquid alloys are carried out by using the density functional theory (DFT) implemented in the Vienna *ab initio* simulation package (VASP) code¹³⁻¹⁵ combined with constant number of particles, constant volume, and constant temperature (NVT) ensembles.¹⁵ The temperature is controlled using the Nosé-Hoover thermostat.^{16, 17} A time-step of 3 fs is used which has been verified to give a stable solution to the equations of the motions of the atoms during the MD simulations. The projector augmented-wave (PAW) method with the Perdew-Burke-Ernzerhof (PBE) form exchange-correlation potentials of general gradient approximation (GGA) is adopted in our simulations. Only the Γ point is considered for sampling the Brillouin zone of the super-cell. A hundred atoms consisting of 80 Cu atoms and 20 Si atoms were randomly put in a cubic box and heated up to 2000 K in order to remove the memory effects from the initial configuration. Periodic boundary conditions are used in the calculations. Then the system is cooled down to the temperatures of 1473, 1373, 1250, 1210,

1175, and 1140 K, successively. Since there is no experiment data on the density of $\text{Cu}_{80}\text{Si}_{20}$ liquid available, the initial atomic number densities in our MD simulations were estimated by the linear combination of the densities of pure liquid Cu and liquid Si, and then adjusted during the MD simulation for different temperatures by varying the box length of the super-cell and keeping the average pressure of the system close to zero (within 0.0 ± 0.5 kB). The corresponding optimized number densities are 0.07732, 0.07709, 0.07689, 0.07684, 0.07596, and 0.07554 $\text{atom}/\text{\AA}^3$ for 1140, 1175, 1210, 1250, 1373, and 1473 K, respectively. At each temperature, the super-cell is equilibrated for 4000 time steps (12 ps). The results of the structural and dynamical properties of $\text{Cu}_{80}\text{Si}_{20}$ liquid alloys are then derived through performing the statistical averages over another 4000 time steps.

The experimental pair-correlation function (PCF), $g(r)$, is obtained by Fourier transformation of the measured total structure factor $S(q)$ using the following equation:

$$g(r) = \frac{\rho(r)}{\rho_o} = 1 + \frac{1}{4\pi r \rho_o} \left[\frac{2}{\pi} \int_0^\infty q [S(q) - 1] \sin(qr) dq \right] \quad (1)$$

where, $\rho(r)$ is the atomic density at a distance r from an average atom located at the origin and ρ_0 is the average atomic density of the material obtained from the simulations.

From the atomic coordinates generated by the *ab initio* MD, the theoretical partial pair-correlation function $g_{\alpha\beta}(r)$ between the atom type α and β can be calculated:

$$g_{\alpha\beta}(r) = \rho_{\alpha\beta}^{-2} \left\langle \sum_i \sum_{j \neq i} \delta(\vec{r}_{i\alpha}) \delta(\vec{r}_{j\beta} - r) \right\rangle \quad (2)$$

where $\rho_{\alpha\beta} = \rho_0 \sqrt{x_\alpha x_\beta}$ corresponding partial density with ρ_0 being the atomic density of the liquid and x_α and x_β being the atomic concentration of the corresponding elements in the liquid. The $g_{\alpha\beta}(r)$ shows the probability of finding β particles around α in the range of r relative to the

probability expected for a completely homogeneous distribution at the same density. Through the total and partial pair-correlation function, the real space local structure of the liquid can be obtained in a statistic manner.

The total structure factor $S(q)$ from the MD simulations were calculated by the Faber-Ziman formalism¹⁸ using the three partial structure factors $S_{\alpha\beta}(q)$, atomic concentration of the elements x_α and x_β , and the q -dependent scattering factors $f_\alpha(q)$ and $f_\beta(q)$ for Cu and Si respectively:

$$S(q)-1 = \frac{x_\alpha^2 f_\alpha^2(q)(S_{\alpha\alpha}(q)-1) + 2x_\alpha x_\beta f_\alpha(q)f_\beta(q)(S_{\alpha\beta}(q)-1) + x_\beta^2 f_\beta^2(q)(S_{\beta\beta}(q)-1)}{(x_\alpha f_\alpha(q) + x_\beta f_\beta(q))^2} \quad (3)$$

The scattering factors $f_\alpha(q)$ and $f_\beta(q)$ are obtained from tabulated data.¹⁹ The partial structure factors, $S_{\alpha\beta}(q)$, are related to the partial pair correlation functions $g_{\alpha\beta}(r)$ by

$$S_{\alpha\beta}(q) = 1 + 4\pi\rho_{\alpha\beta} \int_0^\infty r^2 \frac{\sin qr}{qr} (g_{\alpha\beta}(r) - 1) dr \quad (4)$$

where, the $g_{\alpha\beta}(r)$ can be calculated by the Eq. (2).

The total pair correlation function, $g(r)$, from the *ab initio* MD simulation can then be calculated by the Fourier transformation of structure factor $S(q)$ using the standard transformation techniques as described by Eq. (1).

III. RESULTS AND DISCUSSIONS

A. Pair-correlation functions and structure factors

The total and partial pair-correlation functions $g(r)$ of the liquid $\text{Cu}_{80}\text{Si}_{20}$ are plotted in Fig. 1. The temperatures simulated in this work are 1473, 1373, 1250, 1210, 1200, 1175, and 1140 K, respectively. The experimental data obtained at 1250, 1210, 1175, and 1140 K are given in Fig. 1(a) for comparison. From Fig. 1(a), it can be seen that the agreement between the experiment and simulation is good, with the root mean square error values of the $g(r)$ being 0.1303, 0.1304,

0.1261, and 0.1282 for 1140, 1175, 1210, and 1250 K, respectively. The total pair-correlation function $g(r)$ becomes sharper with decreasing temperature, as expected.²⁰ Because the radius of Si atom is smaller than that of Cu atom, the location of the first peak of $g_{\text{Cu-Si}}(r)$ is obviously smaller than that of $g_{\text{Cu-Cu}}(r)$, as can be inferred from Fig. 1(b) and (c). The other characteristic of the $g_{\text{Si-Si}}(r)$ is the lack of any direct Si-Si bonds with the first peak located within the second shell of the $g(r)$. This would indicate a strong chemical ordering of Cu-Si-Cu triplets in the liquid.

B. Short-range order

The coordination number (N) is derived by integrating the pair-correlation function to its first valley. The total and partial coordination number of liquid $\text{Cu}_{80}\text{Si}_{20}$ alloy from this work is shown in Fig. 2. A linear yet small temperature dependence of all the coordination numbers with temperature is observed. Except for $N_{\text{Si-Si}}$, the other total and partial coordination numbers all increase slightly with the decrease of temperature.

The pair-wise correlations lack the higher order information which may be more informative about chemical and topological ordering. Bond-angle distributions are one means to quantify these higher order correlations. It can be derived by statistically summing the angles between a specific atom and its two neighbor atoms within a cut-off distance, which is determined by the location of the first minimum of $g(r)$. The partial bond-angle distributions of the $\text{Cu}_{80}\text{Si}_{20}$ liquid alloy are plotted in Fig. 3. They are divided into three classes: Cu-(Cu/Si)-Cu, Si-(Cu/Si)-Si, and Cu-(Cu/Si)-Si, respectively. For Cu-Cu-Cu and Cu-Si-Cu, there are two main peaks located at about 57° and 110° (Fig. 3(a) and (b)). This feature is quite close to the bond-angle distributions of liquid and amorphous Cu (60° and 110°).^{21, 22} Those of Cu-Si-Si and Cu-Cu-Si are similar to the curves of Cu-(Si/Cu)-Cu (Fig.3(c) and (d)), but the locations of two peaks are at about 55° and 106° , which are slightly smaller. The plot of Si-Cu-Si (Fig. 3(e))

shows a main peak at around 109° , while that of Si-Si-Si (Fig. 3(f)) appears to be irregular, since there are few Si-Si bonds in the system. This peak at 109° has a strong tetrahedral characteristic of amorphous Si,²³ which is also found in the study of $Al_{1-x}Si_x$.²⁴ Even though the temperature difference is not large, the Si-Cu-Si bond-angle distributions (Fig. 3(e)) show a significant larger dependence than the other bond groups.

The Honeycutt-Andersen index²⁵ is usually used to describe the local poly-types in disordered systems. By examining the bonding around a common pairs of atoms, the HA index provides us with the classification of some specific grouping, such as ISRO, BCC, HCP, and FCC. Adopting the simplified HA index method by Ganesh and Widom,^{22, 26} in this work, we use three digits to describe the common neighbors as shown in Fig. 4. The first digit should be 1 if the root pairs are bonded (i.e., within cut-off radius r_{cut}). The middle digit stands for the number of common neighbors of the root pairs. The last digit shows how many of them are bonded between the common neighbors. The ISRO is characterized by the 155 pairs while the 154 pairs are usually attributed to a distorted icosahedral short-range order. FCC and HCP type-structures are designated as 142 pairs. From Fig. 4 it can be seen that the 155 and 154 pairs increase while the 142 pairs decrease as the temperature is lowered, indicating the development of the icosahedral SRO in the undercooled liquid. Although the population of the 143 pairs is also large, its variation with temperature is small because these pairs can be associated with either distorted icosahedra or distorted closed-packed-structures. Thus, atoms in the icosahedral and distorted icosahedral SROs dominate the local structure of the $Cu_{80}Si_{20}$ liquid alloy. At the same time, there is a noticeable fraction (12-14%) of the FCC/HCP like HA clusters in the liquid. Besides, the fraction of indexes 166 and 144 remains at about 5%, while other indexes 120, 121, 130, 131, 132, 133, 177 (not plotted) are always no more than 3%. Note that the HA index describes only

the configuration of the common neighbors of a pair of atoms and does not give a complete analysis of the polyhedral order around each atom in the system which is discussed below.

Further classification of the polyhedral order is performed using Voronoi Tessellation (VT).^{27, 28} The Voronoi polyhedra (VP) are constructed from all the edges formed from the intersection of the planes halfway between the central atom and all of its neighbors. The VPs are classified based on the number of edges per polyhedral faces; $\langle n_3, n_4, n_5, n_6, \dots, n_i \rangle$, where n_i is the number of the i -edged sides of the polyhedron. For example, the Voronoi indices of perfect icosahedron, FCC, and BCC are $\langle 0,0,12,0 \rangle$, $\langle 0,6,0,8 \rangle$, and $\langle 0,12,0,0 \rangle$, respectively. However, the VPs in a liquid will be distorted from their crystalline counter parts. Therefore we can classify a group of VPs, such as $\langle 0,3,6,4 \rangle$, $\langle 0,3,6,5 \rangle$, $\langle 0,4,4,6 \rangle$, and $\langle 0,4,4,7 \rangle$, as deformed FCC VPs.²⁹

The top 10 representative topological structures of the most frequent clusters and their population that exist in the liquid $\text{Cu}_{80}\text{Si}_{20}$ alloy for the temperatures studied are given in Fig. 5, together with their Voronoi cells. It can be seen that two groups of VPs account for the most VPs in the analysis. One group is the icosahedral $\langle 0,0,12,0 \rangle$, and its distorted variances of $\langle 0,2,8,2 \rangle$, and $\langle 0,1,10,2 \rangle$, while the other group is comprised of deformed FCC polyhedral; $\langle 0,3,6,4 \rangle$, $\langle 0,3,6,5 \rangle$, and $\langle 0,4,4,6 \rangle$. Therefore, the FCC and icosahedral SROs play dominant roles in the liquid $\text{Cu}_{80}\text{Si}_{20}$ alloy according to the Voronoi tessellation analysis. As the temperature is lowered, the icosahedral and FCC-like VPs show a clearly increasing trend. The VPs with CN of 11 and 12 prefer Si centred while others with CN of 13 and 14 are dominated by Cu centers, which can be reasonably attributed to the smaller radius of Si than that of Cu. The result of the Voronoi analysis is consistent with the above HA index analysis but allows for a chemically specific analysis.

We further explored the SRO in the liquid $\text{Cu}_{80}\text{Si}_{20}$ using a recently developed atomic cluster alignment (ACA) method.³⁰ At each temperature, two sets of Cu-centered or Si-centered clusters each contains 2000 clusters up to the first shell from the center atom respectively, are randomly picked up from the molecular dynamics simulation trajectories. The SRO characters of these clusters are classified by two types of alignment schemes. One is the collective-alignment in which all 2000 clusters with the same-type of center atoms are first brought to a common origin then the clusters are rigidly rotated with each other until the sum of mean square distances from the corresponding atoms in different clusters is minimized. The collective-alignment thus gives the probability of the nearest neighbors' locations in both distance and angle from the center atom type. By using a Gaussian smearing scheme to smooth the atomic distribution after the collective alignment, a 3D spatially-resolved distribution function can be generated:

$$D(\vec{r}) = \frac{1}{m} \sum_{i=1}^{m \times n} \left(\frac{\alpha}{\pi} \right)^{3/2} e^{-\alpha \cdot (\vec{r} - \vec{r}_i)^2} \quad (5)$$

where \vec{r}_i is the position vector of atom i , m is the number of the clusters in the alignment and n is the number of atoms in each cluster. In this paper, the parameter α is set to 4.0 \AA^{-2} . The result of such an alignment is a three-dimensional (3D) representation of the average polyhedral SRO.

Another alignment scheme is an individual cluster-template alignment. In this scheme, each cluster in the liquid is aligned with a given template (icosahedra, fcc, bcc, etc.) to identify its order character, and the fraction of each type of SRO in the liquid can thus be classified. Detail procedures of both alignments can be found in Ref 30.

The collective alignment results for $\text{Cu}_{80}\text{Si}_{20}$ distinguished by Cu and Si-centered clusters at different temperatures are plotted in Fig. 6. Both Cu and Si centers exhibit icosahedral-like

five-fold symmetry. This is strong evidence that ISRO dominates the liquid $\text{Cu}_{80}\text{Si}_{20}$ alloy, in agreement with HA-index and Voronoi tessellation analysis.

HA and VP results both indicate that FCC SRO are one of the more populous polyhedral types in the $\text{Cu}_{80}\text{Si}_{20}$ liquid in addition to the ISRO. Given the degree of distortions leading to high variety of polyhedral types, the template cluster-alignment approach provides a more statistically robust means of quantifying the average structure type.³⁰ Four types of SRO templates (FCC, HCP, BCC and icosahedral) are used in the alignment. Since BCC and HCP templates show no significant matching, only the development of ISRO and FCC SRO in the liquid $\text{Cu}_{80}\text{Si}_{20}$ upon cooling are shown in Fig. 7. It can be seen that the population of ISRO clusters is almost twice that of FCC SRO at the highest temperature and increases drastically with the decreasing temperature. On the other hand, FCC SRO increases slightly with cooling and seem to reach a steady value around 1175 K. From Fig. 7(b), it can be readily seen that the FCC clusters prefer Cu centers. However, the icosahedral clusters show no chemical preference (Fig. 7(a)). Unlike the HA, the ACA clearly show that FCC SRO increases as the temperature is lowered. This ACA analysis result indicates that more crystalline like-order is competing with the icosahedral order as the liquid approaches the liquidus.

C. The chemical short-range order

Chemical short-range order (CSRO) in alloys is responsible for the specific concentration and temperature dependence of thermodynamic and structure properties for liquid binary alloys. Warren-Cowley CSRO parameter³¹ is a crude but useful parameter to evaluate the CSRO in disordered system. The Warren-Cowley CSRO parameter α_{ij} , was calculated by using the following equation:

$$\alpha_{ij}=1-N_{ij}/c_jN_{\text{tot}} \quad (6)$$

where N_{ij} and N_{tot} are the partial and total coordination numbers and c_j is the concentration of j particle. The calculated CSRO parameters are given in Table 1. The dependence of the Warren-Cowley parameter on temperature is not significant, consistent with the previous study on CuZr liquid alloys.³² The negative values of $\alpha_{\text{Cu-Si}}$ indicate that there is an affinity between the Cu and Si atoms. The stronger the negative value of α_{ij} , the greater is the CSRO. The relation between like atoms appears to be repulsive according to the Warren-Cowley CSRO parameter analysis. Moreover, $\alpha_{\text{Si-Si}}$ is even larger than $\alpha_{\text{Cu-Cu}}$, indicating the repulsion between Si atoms is relatively stronger, explaining the absence of the first peak of $g_{\text{Si-Si}}(r)$ as discussed above.

D. Dynamical properties

The dynamical properties are important for describing the nucleation and glass-forming process of liquids. The dynamical properties of liquid can be quantified using the mean-square displacement (MSD) as a function of time as given in:

$$\langle R_\alpha^2(t) \rangle = \frac{1}{N_\alpha} \left\langle \sum_{i=1}^{N_\alpha} |R_{i\alpha}(t+\tau) - R_{i\alpha}(\tau)|^2 \right\rangle \quad (7)$$

where N_α is the number of α atoms, $R_{i\alpha}$ is the coordinates of the atom i , and τ is the arbitrary origin of time. In a typical liquid, the MSD is linear with respect to time in the long time limit. The self-diffusion coefficient, D , is dependent on slope of MSD, which can be derived through the Einstein relationship:

$$D = \lim_{t \rightarrow \infty} \langle R_{i\alpha}^2(t) \rangle / 6t \quad (8)$$

As can be inferred from the nearly linear behavior of the MSD depicted in Fig. 8, the simulations of the liquid states is well behaved for $\text{Cu}_{80}\text{Si}_{20}$. The diffusivity of the liquid decreases with temperature as expected. The self-diffusion coefficients as the functions of temperature are given in the right-hand side panels of Fig. 8. The error bars in the plot was

calculated by dividing the total 4000 MD steps into four 1000 MD steps. The total diffusion coefficient decreased from 0.25×10^{-4} to 0.09×10^{-4} cm²/s with decreasing temperature. The diffusion coefficient of copper decreased from 0.26×10^{-4} to 0.09×10^{-4} cm²/s, while that of silicon from 0.20×10^{-4} to 0.07×10^{-4} cm²/s, as temperature decreases. The diffusion coefficient of copper in the Cu₈₀Si₂₀ liquid alloy in this work is about 0.1×10^{-4} cm²/s smaller than that of pure copper liquid under the same temperature.³³ It can be interpreted by that the Si addition will reduce the diffusivity of the system, which is common in the Si added metallic liquids. The decrease of diffusion constant as temperature decreases as shown in Fig. 8 may be partially attributed to the increase of icosahedral SRO in the liquid upon cooling. It has been shown in the literature that the increase of icosahedral SRO can slow down the dynamics of liquid and leading to glass formation.^{2, 34}

The relation between the self-diffusion coefficients and temperature obeys an Arrhenius relationship:

$$D = D_0 e^{-\frac{E_a}{k_B T}} \quad (9)$$

where E_a is the activation energy, T is the temperature, D_0 is the pre-exponential factor, and k_B is the Boltzmann constant. In the right-hand panels of Fig. 8, the self-diffusion coefficients fit within acceptable tolerance to equation (9). The E_a and D_0 were derived by fitting $\ln D$ by $1/T$. The activation energy E_a is 38.715 kJ/mol, 37.972 kJ/mol, and 42.540 kJ/mol for the liquid, the Cu and Si self-diffusion, respectively. The pre-exponential factor D_0 is 5.768×10^{-8} m²/s and 7.729×10^{-8} m²/s, for Cu and Si respectively. The activation energy of Si is larger than that of Cu, indicating that the bonding of Si and its surrounding atoms are stronger than that of Cu. The E_a value of Cu in this study is a little smaller than that of Cu liquid 40.4 kJ/mol.³³

IV. CONCLUSIONS

In summary, the local structure and dynamical properties of liquid $\text{Cu}_{80}\text{Si}_{20}$ alloy have been studied using *ab initio* molecular dynamics simulations validated using X-ray diffraction. The calculated pair-correlation functions compared well with the experimental results. We found that the coordination number shows a linear relationship with temperature. Honeycutt-Andersen index analysis, Voronoi tessellation analysis, and a newly developed atomic cluster alignment method are carried out to quantify the local atomic environment of the liquid. The ACA provides a 3D description of the average SRO. The ISRO and FCC SRO are the dominant polyhedral order in the liquid. The degree of ISRO increases with the decreasing of temperature, while the FCC SRO also increases with cooling indicating that crystalline order begins to compete with icosahedral order as the liquid approaches its liquidus. Finally, the CSRO and the dynamical properties, such as the MSD and self-diffusion coefficient, are investigated as well. The result of the CSRO shows that there exists affinity between Cu and Si atoms, while the relationship between the same species of atoms is repulsive. The repulsion between Si atoms is much stronger than that between Cu atoms. The linearity of the MSD results demonstrate that the liquid is well behaved so that the self-diffusion coefficient can be fitted to the Arrhenius relationship and the activation energy of Cu is in reasonable agreement with previous liquid study.

ACKNOWLEDGEMENTS

One of the authors (S.Y.W.) is partially supported by the NSF of China (Grant No. 10974029), National Basic Research Program of China (No. 2012CB934303) Doctoral Fund of Ministry of Education of China (No. 20100071110025). X. W. F. acknowledges the support from China Scholarship Council for the Postgraduate Scholarship Program (File NO.2008634035) and

Z. J. D. acknowledges the National Natural Science Foundation of China (Grant No. 10874160) and the '111' project. Ames Laboratory is operated for the U.S. Department of Energy by Iowa State University under Contract No.DE-AC02-07CH11358. This work is supported by the Director for Energy Research, Office of Basic Energy Sciences, Materials Science and Engineering Division including a grant of computer time at the National Energy Research Supercomputing Centre (NERSC) in Berkeley. Use of the Advanced Photon Source was supported by the U. S. Department of Energy, Office of Science, Office of Basic Energy Sciences, under Contract No. DE-AC02-06CH11357.

- ¹ D. Holland-Moritz, T. Schenk, P. Convert, T. Hansen, and D. M. Herlach, *Meas. Sci. Technol.* **16**, 372 (2005).
- ² K. F. Kelton, G. W. Lee, A. K. Gangopadhyay, R. W. Hyers, T. J. Rathz, J. R. Rogers, M. B. Robinson, and D. S. Robinson, *Phys. Rev. Lett.* **90**, 195504 (2003).
- ³ M. J. Kramer, *J. Appl. Crystallogr.* **40**, 77 (2007).
- ⁴ B. J. Alder and T. E. Wainwright, *J. Chem. Phys.* **31**, 459 (1959).
- ⁵ R. L. McGreevy and L. Pusztai, *Mol. Simul.* **1**, 359 (1988).
- ⁶ H. Okamoto, *Desk Handbook: Phase Diagrams for Binary Alloys* (ASM International, 2000).
- ⁷ O. Fabrichnaya and A. Prince, in *Noble Metal Ternary Systems: Phase Diagrams, Crystallographic and Thermodynamic Data*, edited by G. Effenberg and S. Ilyenko, Vol. 11B.
- ⁸ L. Margulies, M. J. Kramer, R. W. McCallum, S. Kycia, D. R. Haefner, J. C. Lang, and A. I. Goldman, *Rev. Sci. Instrum.* **70**, 3554 (1999).
- ⁹ A. P. Hammersley, S. O. Svensson, M. Hanfland, A. N. Fitch, and D. Häusermann, *High Pressure Res.* **14**, 235 (1996).
- ¹⁰ Y. Waseda and M. Ohtani, *Phys. Status Solidi B* **62**, 535 (1974).
- ¹¹ T. Egami and S. J. L. Billinge, *Underneath the Bragg Peaks: Structural Analysis of Complex Materials*. (Elsevier, 2003).
- ¹² O. J. Eder, E. Erdpresser, B. Kunsch, H. Stiller, and M. Suda, *J Phys. F: Metal Phys.* **10**, 183 (1980).
- ¹³ G. Kresse and J. Hafner, *Phys. Rev. B* **47**, 558 (1993).
- ¹⁴ G. Kresse, Technische Universität Wien, 1993.
- ¹⁵ G. Kresse and J. Furthmüller, *Comput. Mater. Sci.* **6**, 15 (1996).
- ¹⁶ S. Nosé, *J. Chem. Phys.* **81**, 511 (1984).
- ¹⁷ W. G. Hoover, *Phys. Rev. A* **31**, 1695 (1985).
- ¹⁸ P. A. Egelstaff, *An introduction to the liquid state* (Oxford, Clarendon, 1992).
- ¹⁹ A. Prince and P. Liang, *Silver-Gold-Silicon* (VCH Publishers, New York, 1995).
- ²⁰ Y. Waseda, *The Structure of Non-Crystalline Materials-Liquids and Amorphous Solids* (McGraw-Hill, New York, 1981).
- ²¹ A. Di Cicco and A. Trapananti, *J. Non-Cryst. Solids* **353**, 3671 (2007).
- ²² P. Ganesh and M. Widom, *Phys. Rev. B* **74**, 134205 (2006).
- ²³ M. Ishimaru, *J. Phys.: Condens. Matter* **13**, 4181 (2001).
- ²⁴ S. Y. Wang, C. Z. Wang, C. X. Zheng, and K. M. Ho, *J. of Non-Cryst. Solids* **355**, 340 (2009).
- ²⁵ J. D. Honeycutt and H. C. Andersen, *J. Phys. Chem.* **91**, 4950 (1987).
- ²⁶ P. Ganesh and M. Widom, *Phys. Rev. B* **77**, 014205 (2008).
- ²⁷ J. L. Finney, *Proc. R. Soc. A* **319**, 479 (1970).
- ²⁸ J. L. Finney, *Nature* **266**, 309 (1977).
- ²⁹ P. R. ten Wolde, M. J. Ruiz-Montero, and D. Frenkel, *J. Chem. Phys.* **104**, 9932 (1996).
- ³⁰ X. W. Fang, C. Z. Wang, Y. X. Yao, Z. J. Ding, and K. M. Ho, *Phys. Rev. B* **82**, 184204 (2010).
- ³¹ B. E. Warren, B. L. Averbach, and B. W. Roberts, *J. Appl. Phys.* **22**, 1493 (1951).
- ³² N. Jakse and A. Pasturel, *Phys. Rev. B* **78**, 214204 (2008).
- ³³ J. Mei and J. W. Davenport, *Phys. Rev. B* **42**, 9682 (1990).
- ³⁴ W. K. Luo, H. W. Sheng, F. M. Alamgir, J. M. Bai, J. H. He, and E. Ma, *Phys. Rev. Lett.* **92**, 145502 (2004).

Figure and Table Captions:

FIG. 1: Comparison the total pair-correlation functions between measurement and simulation and the calculated partial pair-correlation functions of the liquid $\text{Cu}_{80}\text{Si}_{20}$ alloy at different temperatures.

FIG. 2: The average and partial coordination number of liquid $\text{Cu}_{80}\text{Si}_{20}$ alloy.

FIG.3: Calculated partial bond-angle distribution functions of liquid $\text{Cu}_{80}\text{Si}_{20}$ alloy. (a) Cu-Cu-Cu; (b) Cu-Si-Cu; (c) Cu-Si-Si; (d) Cu-Cu-Si; (e) Si-Cu-Si; (f) Si-Si-Si.

FIG. 4: The top 4 most populated HA indices in liquid $\text{Cu}_{80}\text{Si}_{20}$ alloy as the function of temperature.

FIG. 5: The result of the Voronoi tessellation analysis of liquid $\text{Cu}_{80}\text{Si}_{20}$ alloy. The clusters and Voronoi cells are given in the right panel: (a) icosahedral like; (b) FCC like; (c) unclassified.

FIG. 6: The collective alignment results for $\text{Cu}_{80}\text{Si}_{20}$ at different temperatures. Clusters in the upper panel represent the Cu centered (blue) ones and those in the lower panel stand for the Si centered (yellow) ones. The iso value is set to be 0.42 \AA^{-3} .

FIG. 7: Population analysis by using the individual cluster-template alignment. (a) Population of ICO SRO in whole system, in Cu centered clusters, and Si centered clusters, respectively. (b) Population of FCC SRO in whole system, in Cu centered clusters, and Si centered clusters, respectively. The populations are normalized to the corresponding number of atoms (i.e., 100 for total, 80 for Cu-centered and 20 for Si-centered) in the system respectively.

FIG. 8: The MSD and self-diffusion coefficient of $\text{Cu}_{80}\text{Si}_{20}$ at different temperature. The red lines are the fitting lines.

Table 1. The calculated Warren-Cowley CSRO parameter α_{ij}

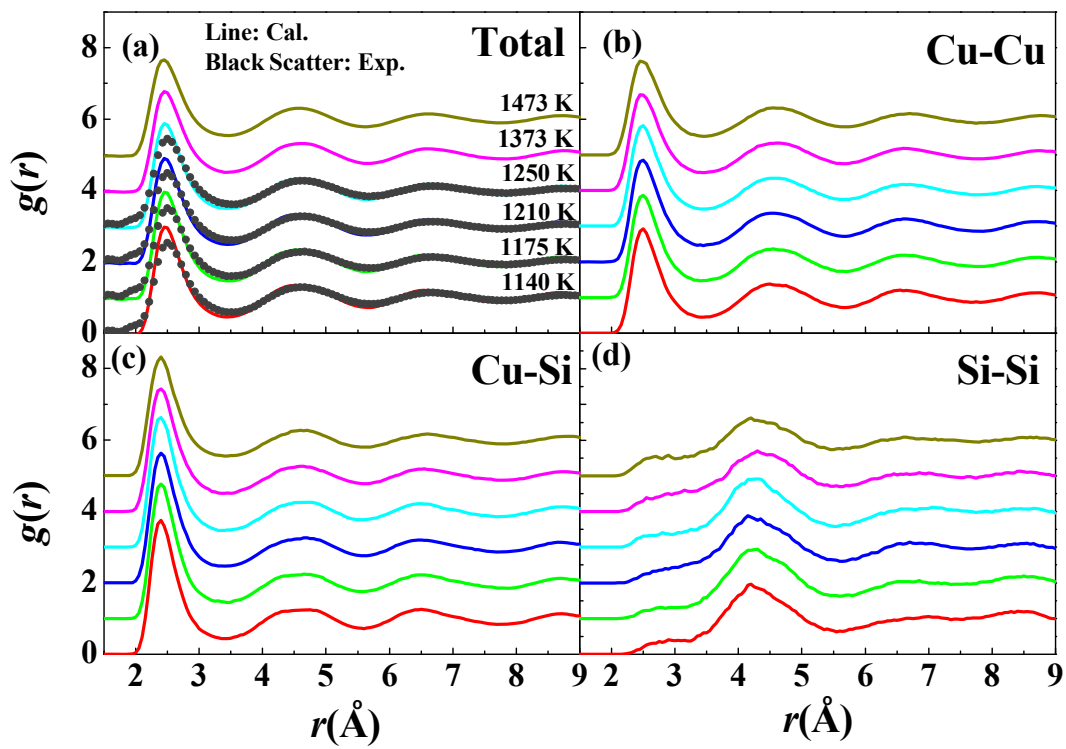


FIG. 1: Comparison the total pair-correlation functions between measurement and simulation and the calculated partial pair-correlation functions of the liquid $\text{Cu}_{80}\text{Si}_{20}$ alloy at different temperatures.

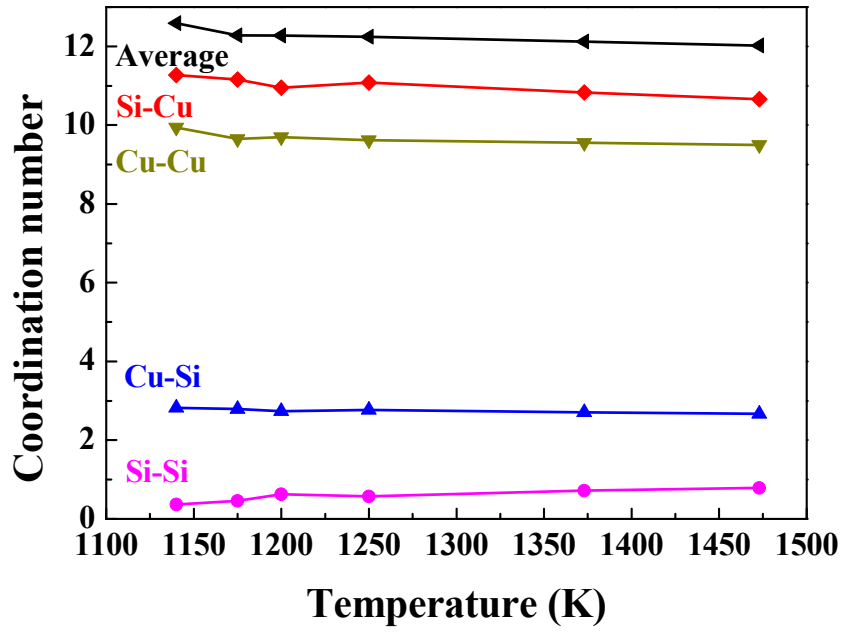


FIG. 2: The average and partial coordination number of liquid $\text{Cu}_{80}\text{Si}_{20}$ alloy.

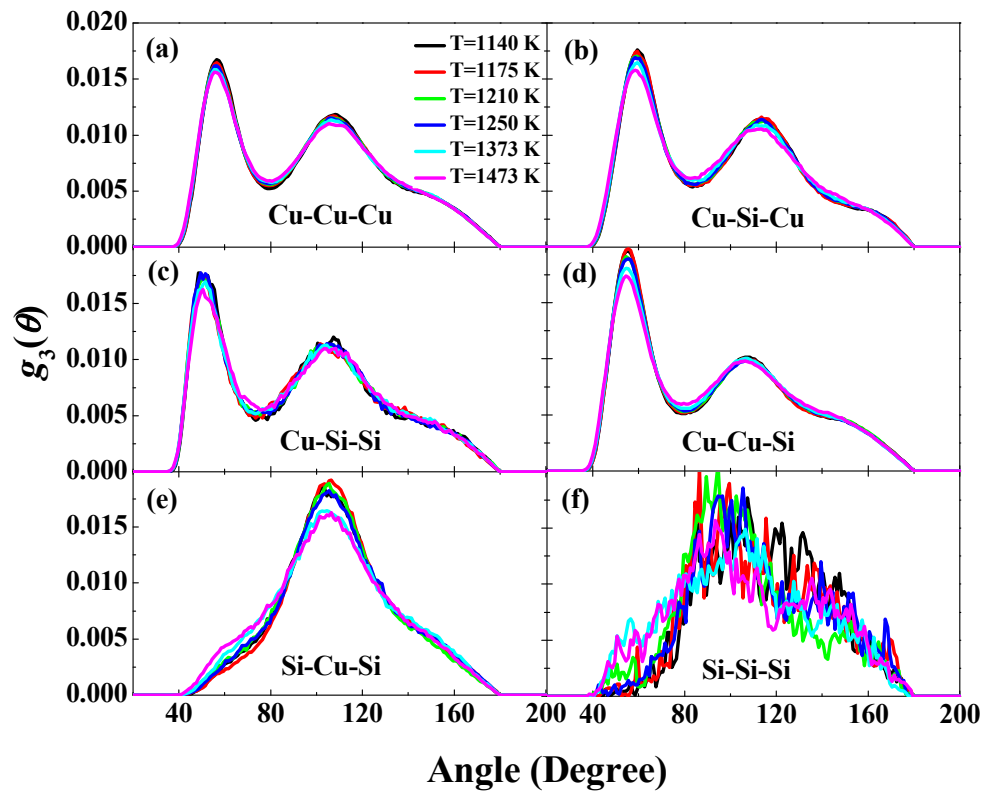


FIG. 3: Calculated partial bond-angle distribution functions of liquid $\text{Cu}_{80}\text{Si}_{20}$ alloy. (a) Cu-Cu-Cu; (b) Cu-Si-Cu; (c) Cu-Si-Si; (d) Cu-Cu-Si; (e) Si-Cu-Si; (f) Si-Si-Si.

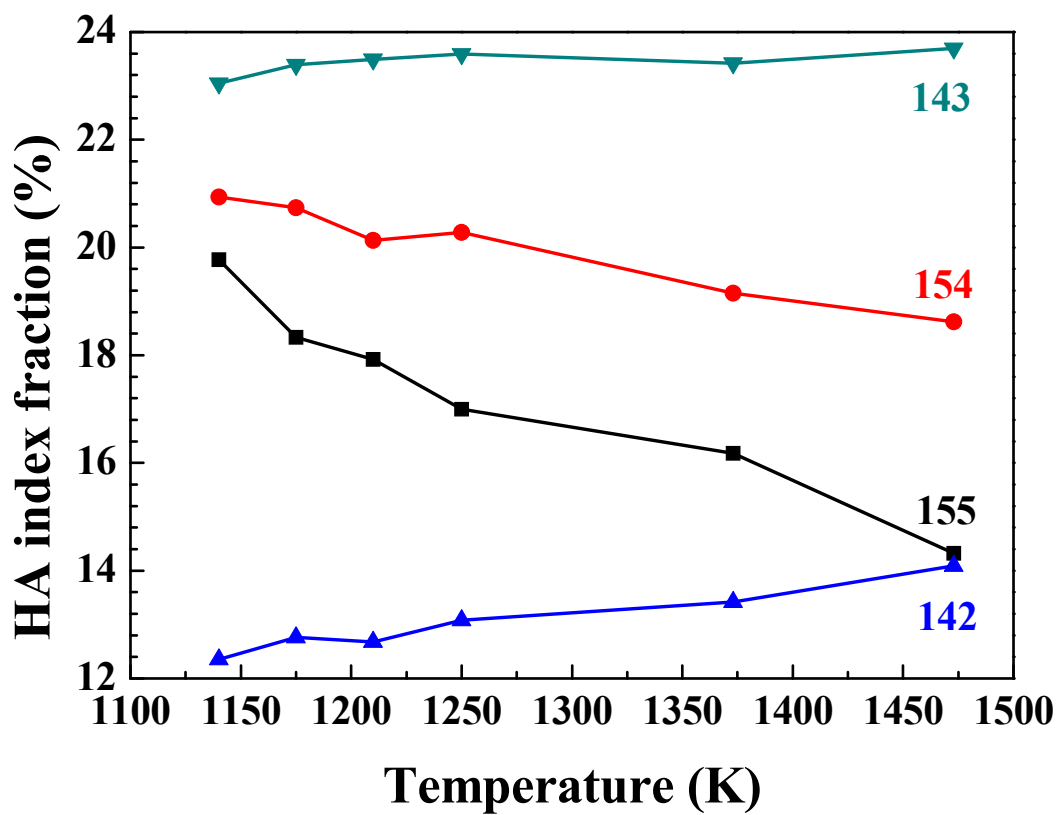


FIG. 4: The top 4 most populated HA indices in liquid $\text{Cu}_{80}\text{Si}_{20}$ alloy as the function of temperature.

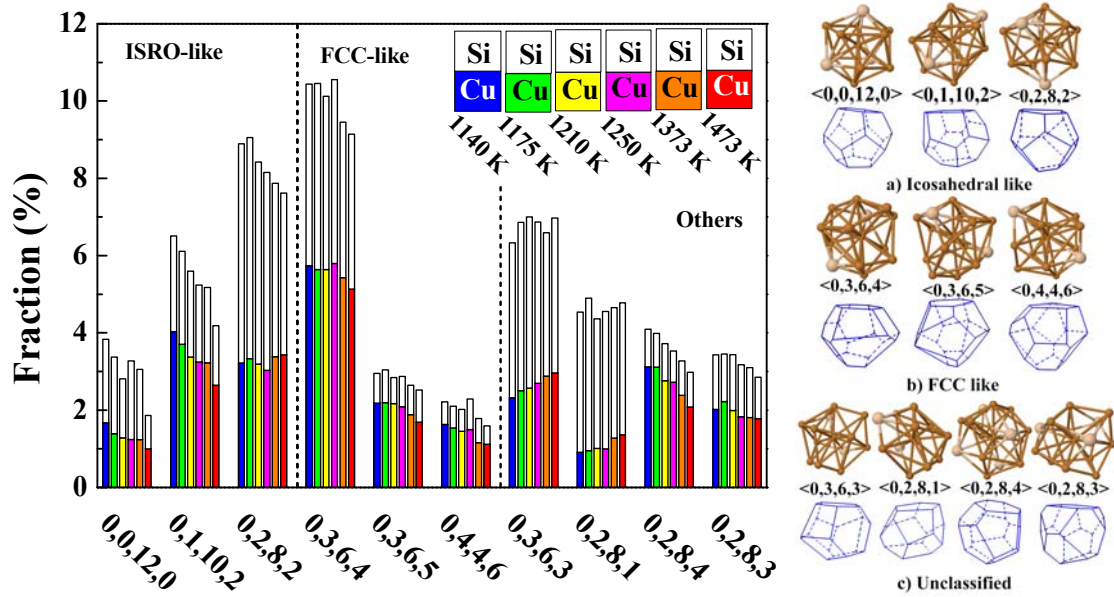


FIG. 5: The result of the Voronoi tessellation analysis of liquid $\text{Cu}_{80}\text{Si}_{20}$ alloy. The clusters and Voronoi cells are given in the right panel: (a) icosahedral like; (b) FCC like; (c) unclassified.

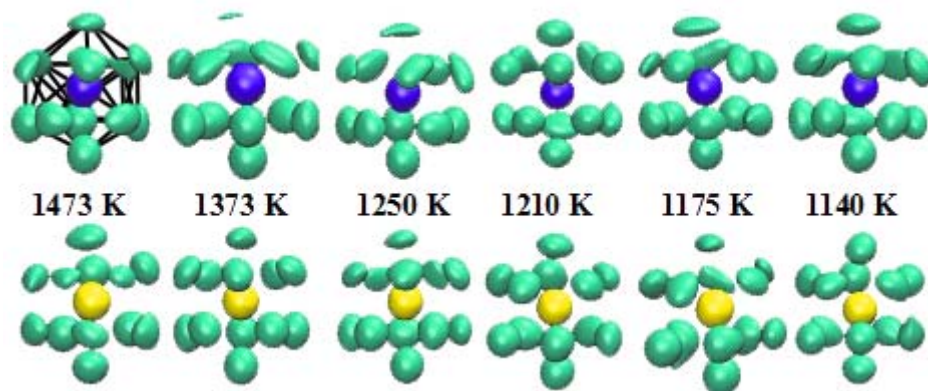


FIG. 6: The collective alignment results for $\text{Cu}_{80}\text{Si}_{20}$ at different temperatures. Clusters in the upper panel represent the Cu centered (blue) ones and those in the lower panel stand for the Si centered (yellow) ones. The iso value is set to be 0.42 \AA^{-3} .

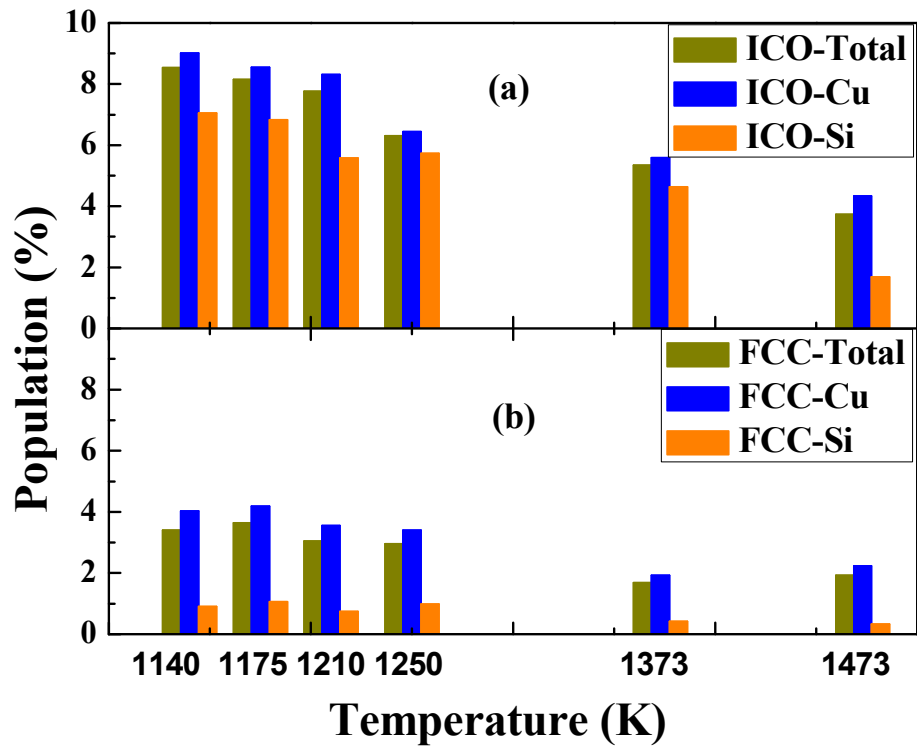


FIG. 7: Population analysis by using the individual cluster-template alignment. (a) Population of ICO SRO in whole system, in Cu centered clusters, and Si centered clusters, respectively. (b) Population of FCC SRO in whole system, in Cu centered clusters, and Si centered clusters, respectively. The populations are normalized to the corresponding number of atoms (i.e., 100 for total, 80 for Cu-centered and 20 for Si-centered) in the system respectively.

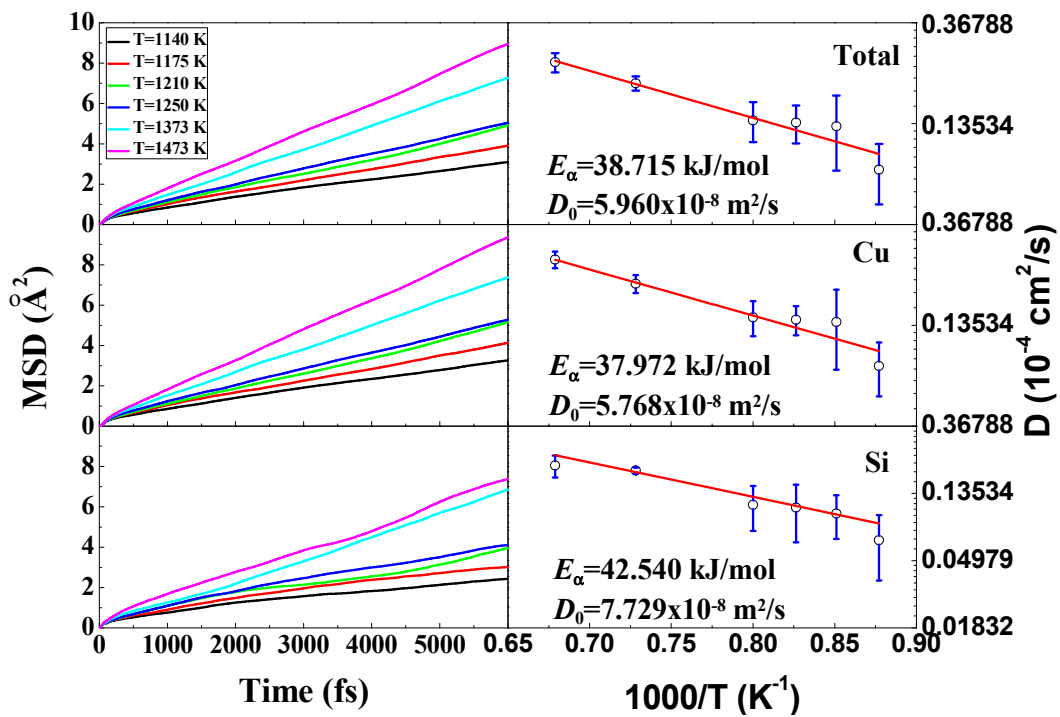


FIG. 8: The MSD and self-diffusion coefficient of $\text{Cu}_{80}\text{Si}_{20}$ at different temperature. The red lines are the fitting lines.

Table 1. The calculated Warren-Cowley CSRO parameter α_{ij}

T (K)	Cu-Si	Cu-Cu	Si-Si
1140	-0.11901	0.01317	0.85443
1175	-0.12138	0.01771	0.81270
1210	-0.10129	0.01182	0.74328
1250	-0.11784	0.01757	0.76716
1373	-0.10522	0.01506	0.70297
1473	-0.09696	0.01206	0.67138